

Valley splitting in Si quantum dots embedded in SiGe

S. Srinivasan,^{1,2} G. Klimeck,^{1,2} and L. P. Rokhinson^{2,3}

¹*Network for Computational Nanotechnology, Purdue University, West Lafayette, Indiana 47907 USA*

²*Birk Nanotechnology Center, Purdue University, West Lafayette, Indiana 47907 USA*

³*Department of Physics, Purdue University, West Lafayette, Indiana 47907 USA*

We examine energy spectra of Si quantum dots embedded into $\text{Si}_{0.75}\text{Ge}_{0.25}$ buffers using atomistic numerical calculations for dimensions relevant to qubit implementations. The valley degeneracy of the lowest orbital state is lifted and valley splitting fluctuates with monolayer frequency as a function of the dot thickness. For dot thicknesses ≤ 6 nm valley splitting is found to be $> 150 \mu\text{eV}$. Using the unique advantage of atomistic calculations we analyze the effect of buffer disorder on valley splitting. Disorder in the buffer leads to the suppression of valley splitting by a factor of 2.5, the splitting fluctuates with $\approx 20 \mu\text{eV}$ for different disorder realizations. Through these simulations we can guide future experiments into regions of low device-to-device fluctuations.

Understanding and design of silicon nanometer-scaled electronic devices has regained significant interest. This interest is sparked by the experimental progress that enabled the reproducible construction of geometries in which electrons are confined in three dimensions to length scales of a few nanometers and the potential applications of this technology to ultra-scaled traditional CMOS devices. Emerging application of Si nanostructures for qubit implementations due to long spin relaxation times[1, 2, 3] imposes additional stringent requirements on energy spectrum engineering, including the precise control of valley degeneracy. The six-fold valley degeneracy of bulk Si is reduced to two-fold degeneracy when electrons are confined to two dimensions (2D), such as at Si/SiO₂ interface in mainstream MOS-FETs. Already decades ago it was recognized that there is a small splitting between the two valleys in the lowest subband[4]. Recently, calculations predicted that valley splitting in narrow (few nm) SiGe/Si/SiGe quantum wells can be of the order of 10-100 meV and should fluctuate rapidly with the well thickness[5, 6, 7, 8]. However, experiments[9, 10, 11] produced valley splitting about 2 orders of magnitude smaller than that prediction, which has been explained[12] by the disorders of the Si/SiGe interface and in the SiGe buffer. The experiments[13] and theoretical methods indicated that additional spatial confinement will minimize the role of interface disorder and increase valley splitting. In this paper we investigate the role of SiGe buffer disorder on valley splitting and answer the fundamental question of the size and controllability of valley splitting for relevant experimental structures.

Three dimensional (3D) confinement of electrons can be achieved by various techniques. Electrostatic surface gating of 2D gas provides relatively weak and smooth spatial confinement potentials. In contrast, 3D confinement by Si/SiO₂ interface produces sharp potential with Coulomb energies approaching room temperature[14, 15] and large valley splitting[16]. Recently, an alternative approach to 3D confinement has been demonstrated with an advantage of lithographically defined epitaxial Si/SiGe interfaces using post-fabrication regrowth[17]. In this

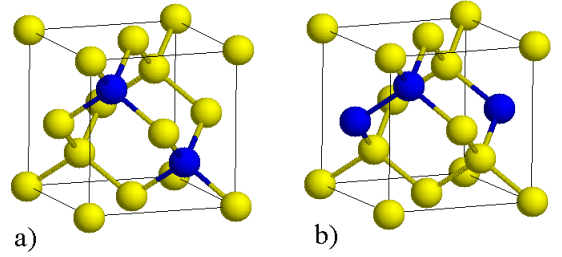


FIG. 1: Placement of Si (yellow) and Ge (blue) atoms in a) fully ordered (Si-Ge and Si-Si bonds) and b) partially ordered (Si-Ge, Ge-Ge and Si-Si bonds) 8-atom supercells.

case spurious charging effects[18], related to the traps in SiO₂ or unpassivated interface can be avoided, yet retaining sharp confining potential. We will simulate such defined Si nanostructures in SiGe buffers and explore sizes relevant for qubit implementations. Simulation capabilities to represent structures containing 10 million atoms explicitly enable the atomic representation of the dot, interfaces and the SiGe buffer. Atomistic simulations also present a unique opportunity to vary the amount of the buffer disorder in order to attain detailed understanding of the physics of valley splitting, including its magnitude and fluctuations. The valley splitting is primarily defined by the smallest dimension of the device and our conclusions are applicable to any Si nanostructure defined from SiGe/Si/SiGe quantum wells.

Calculations of the energy spectrum are performed using the NEMO-3D general purpose code, which represents each atom in the domain explicitly. The theory underlying the tool and its relevant benchmarks are given in Refs [19, 20]. The structure is defined on the relaxed (001) $\text{Si}_{0.75}\text{Ge}_{0.25}$ substrate and the Keating valence-force field model is used to adjust atomic positions to minimize the strain energy. Calculations of electronic structure are based on the 20 band $sp^3d^5s^*$ tight-binding model. The quantum dot was modeled as a $l_x \times l_y \times l_z$ rectangle grown on 37 nm-thick substrate and embedded

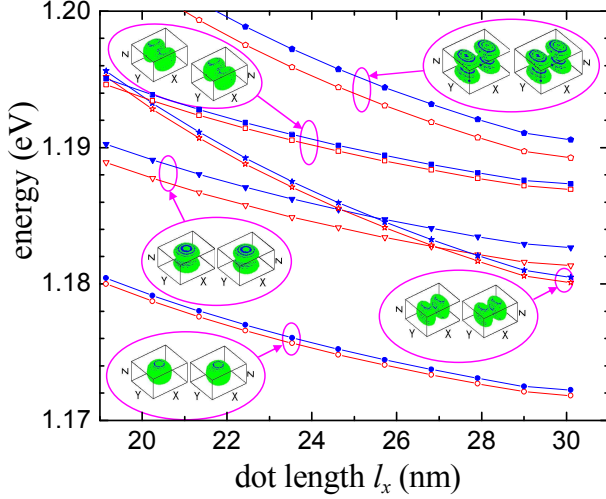


FIG. 2: Energy levels in $l_x \times 20 \text{ nm} \times 10 \text{ nm}$ Si dot embedded into ordered $\text{Si}_{0.75}\text{Ge}_{0.25}$ buffer. Energies are referenced to the valence band Γ_v^8 point. Inserts show spatial distribution of wavefunctions for the lowest levels.

into 27 nm-thick $\text{Si}_{0.75}\text{Ge}_{0.25}$ buffer, $l_z < l_x, l_y$, where z is along the growth direction. We investigated the influence of the buffer thickness on electronic structure, there were no significant changes for substrates $t_s > 30 \text{ nm}$ and buffers $t_b > 20 \text{ nm}$.

For 25% Ge we can generate various placements of Ge atoms in the $\text{Si}_{0.75}\text{Ge}_{0.25}$ buffer, with fully ordered containing only Si-Ge bonds, partially ordered containing single Ge-Ge bond per 8-atom supercell in a fixed position, and disordered having random placement of Ge atoms retaining 25% composition, see schematic in Fig. 1.

We start with the analysis of energy levels and valley splitting in a dot embedded into a fully ordered buffer. Evolution of energy levels for a $l_x \times 20 \text{ nm} \times 10 \text{ nm}$ dot is shown in Fig. 2 (the actual dot thickness $l_z = 9.85 \text{ nm} = 72$ monolayers). All levels come in pairs, both levels in the pair having similar wavefunction envelopes (each level is also double spin-degenerate, which has been confirmed by calculations and will be ignored for the rest of the paper). The 3D representations of the envelope wavefunctions at 20% value are shown for the lowest 6 levels. The two lowest levels have similar s -type wavefunctions and represent the same orbital state with different valley number. The energy difference between them we call valley splitting Δ_v^0 . The next two levels have one node and belong to the next orbital state. For $l_x < 25 \text{ nm}$ the p_z -type state has lower energy than p_x - and p_y -type states due to the combination of sizes and effective mass anisotropy. The p_x -type level has the highest sensitivity to l_x , as expected, and for $l_x > 26 \text{ nm}$ its energy becomes lower than that of the p_z -type state. Energy separation between the ground and the first excited orbital states $\delta E \approx 8 - 10 \text{ meV}$ is large enough to restrict qubit Hilbert

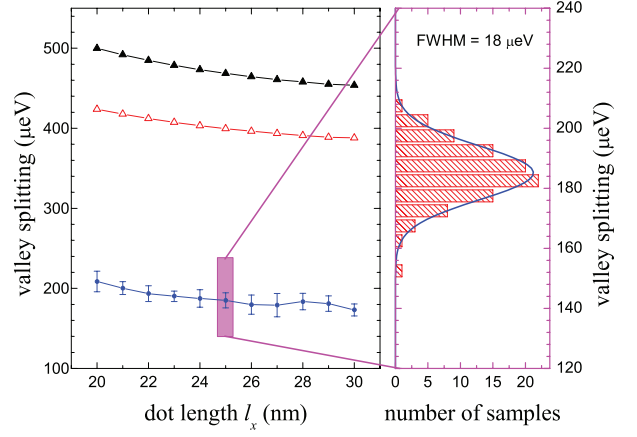


FIG. 3: Valley splitting for the lowest orbital level as a function of the dot size for ordered (black), partially ordered (red) and disordered (blue) $\text{Si}_{0.75}\text{Ge}_{0.25}$ buffer. Bars indicate std deviation for each point. An example of valley splitting distribution for 100 realizations of buffer disorder is shown in the histogram for $l_x = 25 \text{ nm}$, blue curve is the Gaussian fit.

space to the lowest orbital state at low temperatures.

Valley mixing results from superposition of two counter-propagating waves reflected from the opposite Si/SiGe heterointerfaces of the dot. The phase difference of the two waves depends on the details of the interface. The strength of the mixing depends on the amplitude of the wavefunctions at the interfaces, $\Delta_v \propto |\chi(l_b)|^2$, where $\chi(l_b)$ is the value of the envelope of the electron wavefunction at the dot boundary[7]. For p_z -type and d_z -type (top curve in Fig. 2) states wavefunctions are pushed toward z -heterointerface and valley splitting for these state are significantly larger than for the ground and p_x - or p_y -type states.

The most interesting question which can be uniquely studied by atomistic calculations is the role of buffer disorder. In Fig. 3 valley splitting of the ground level is plotted for a $l_x \times 20 \text{ nm} \times 10 \text{ nm}$ dot as a function of the dot size l_x for fully ordered, partially ordered and completely disordered buffer. For fully ordered buffer the valley splitting is $\sim 0.5 \text{ meV}$, consistent with analytical calculations. The value does not change significantly with the dot size, which confirms that valley splitting is primarily determined by the smallest dimension. For partially ordered buffers we see a reduction of Δ_v^0 by 10%, while for fully disordered buffer Δ_v^0 is reduced 2.5 times to $\sim 0.2 \text{ meV}$. To investigate fundamental reproducibility of Δ_v^0 we performed calculations for 100 realizations of the buffer disorder for each point. The histogram of Δ_v^0 for $l_x = 25 \text{ nm}$ dot is plotted in the right frame. The distribution is Gaussian, with standard deviation of $9.4 \mu\text{eV}$, which is $\sim 5\%$ of Δ_v^0 . The bars on the main plot indicate standard deviation for other dot sizes.

Inter-valley mixing is very sensitive to the smallest dimension of the dot, l_z , and fluctuates with a monolayer

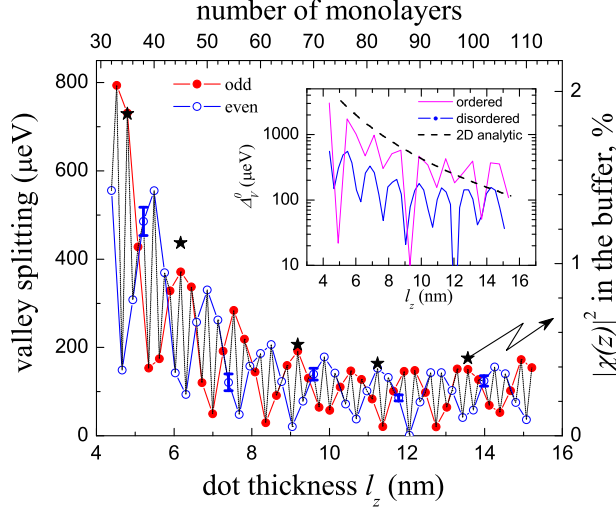


FIG. 4: Valley splitting for the lowest orbital level of $25 \text{ nm} \times 20 \text{ nm} \times l_z \text{ nm}$ Si dot as a function of the dot thickness in monolayers (ML). l_z is calculated using $1 \text{ ML} \approx 0.13707 \text{ nm}$. Thin line connects points 1 ML apart, thick lines connect points 2 MLs apart (open dots for even MLs and solid dots for odd MLs). Bars indicate std deviations for different disorder realizations. Stars show percent of the wavefunction penetrating into the buffer in z direction. In the inset Δ_v^0 for ordered and disordered buffers are plotted. Dashed line is Δ_v^0 obtained analytically for the 2D case.

(ML) frequency $\Delta_v \propto \cos(k_0 l_z)$, where $k_0 = 0.82(2\pi/a)$ is the center of the valleys and a is the lattice constant. Valley splitting as a function of l_z with ML resolution is plotted in Fig. 4 (black line), and bars indicate standard deviation for different disorder realizations. It has been noted that QWs with odd and even number of MLs belong to different symmetry classes[7]. Indeed, if we connect Δ_v^0 for even and odd number of MLs we obtain two similar curves which fluctuate with a period of ≈ 8 MLs and are out-of-phase with each other. The value of $\Delta_v^0(l_z)$ for the dot embedded into a disordered buffer is reduced by a factor of 2.5, as shown in the inset. For comparison we also plot valley splitting calculated for the 2D QW using envelope function method[7] (dashed line), which coincides with our calculations for the ordered buffer. Saturation of valley splitting for large l_z , compared with the $1/l_z^3$ analytical dependence, is due to an additional lateral confinement. In Fig. 4 stars indicate percentage of the wavefunction $|\chi(z)|^2$ which penetrates the buffer above and below the dot, the envelope of Δ_v^0 follows $|\chi(z)|^2$ as a function of l_z .

To summarize, we calculate energy levels and valley splitting for a small Si dot embedded in a disordered $\text{Si}_{0.75}\text{Ge}_{0.25}$ buffer. We find that buffer disorder leads to the suppression of valley splitting by ~ 2.5 and actual

values fluctuate with standard deviation of $\sim 20 \mu\text{eV}$. At the same time disorder limits the lowest valley splitting, which can reach zero for a perfectly ordered buffer for some dot thicknesses, and dots with valley splitting $> 150 \mu\text{eV}$ can be predictably designed from narrow QW ($l_z \leq 6 \text{ nm}$).

The work was supported by ARO/LPS Award No. W911NF-05-1-0437. The use of nanoHUB.org computational resources operated by the Network for Computational nanotechnology funded by NSF is acknowledged.

-
- [1] B. Kane, Nature (London) **393**, 133 (1998).
 - [2] Z. Wilamowski, W. Jantsch, H. Malissa, and U. Rössler, Phys. Rev. B **66**, 195315 (2002).
 - [3] A. Tyryshkin, S. Lyon, W. Jantsch, and F. Schäffler, Phys. Rev. Lett. **94**, 126802 (2005).
 - [4] T. Ando, A. B. Fowler, and F. Stern, Rev. of Mod. Phys. **54**, 437 (1982).
 - [5] T. B. Boykin, G. Klimeck, M. A. Eriksson, M. Friesen, S. N. Coppersmith, P. von Allmen, F. Oyafuso, and S. Lee, Appl. Phys. Lett. **84**, 115 (2004).
 - [6] T. B. Boykin, G. Klimeck, M. Friesen, S. N. Coppersmith, P. von Allmen, F. Oyafuso, and S. Lee, Phys. Rev. B **70**, 165325 (2004).
 - [7] M. O. Nestoklon, L. E. Golub, and E. L. Ivchenko, Phys. Rev. B **73**, 235334 (2006).
 - [8] M. Friesen, S. Chutia, C. Tahan, and S. N. Coppersmith, Phys. Rev. B **75**, 115318 (2007).
 - [9] P. Weitz, R. Hauga, K. V. Klitzing, and F. Schäffler, Surf. Sci. **361/362**, 542 (1996).
 - [10] S. Koester, K. Ismail, and J. Chu, Semicond. Sci. Technol. **12**, 384 (1997).
 - [11] K. Lai, W. Pan, D. C. Tsui, S. Lyon, M. Mühlberger, and F. Schäffler, Phys. Rev. Lett. **93**, 156805 (2004).
 - [12] N. Kharche, M. Prada, T. B. Boykin, and G. Klimeck, Appl. Phys. Lett. **90**, 092109 (2007).
 - [13] S. Goswami, K. Slinker, M. Friesen, L. McGuire, J. Truitt, C. Tahan, L. Klein, J. Chu, P. Mooney, D. V. der Weide, et al., Nat. Phys. **3**, 41 (2007).
 - [14] Y. Takahashi, M. Nagase, H. Namatsu, K. Kurihara, K. Iwdate, Y. Nakajima, S. Horiguchi, K. Murase, and M. Tabe, Electronics Letters **31**, 136 (1995).
 - [15] L. Zhuang, L. Guo, and S. Y. Chou, Appl. Phys. Lett. **72**, 1205 (1998).
 - [16] L. P. Rokhinson, D. C. Tsui, L. N. Pfeiffer, and K. W. West, Superlattices Microstruct. **32**, 99 (2002), cond-mat/0303011.
 - [17] X.-Z. Bo, L. Rokhinson, N. Yao, D. Tsui, and J. Sturm, J. Appl. Phys. **100**, 94317 (2006).
 - [18] L. P. Rokhinson, L. J. Guo, S. Y. Chou, and D. C. Tsui, Appl. Phys. Lett. **76**, 1591 (2000).
 - [19] G. Klimeck, F. Oyafuso, T. Boykin, R. Bowen, and P. von Allmen, Comput. Model. Eng. Sci. pp. 601 – 42 (2002).
 - [20] G. Klimeck, S. Ahmed, H. Bae, N. Kharche, S. Clark, B. Haley, S. Lee, M. Naumov, H. Ryu, F. Saied, et al., IEEE Trans. Electron. Devices pp. 2079 – 89 (2007).